# An In Vitro Study of the Onset of Turbulence in the Sinus of Valsalva

Jon A. Peacock

**During systole a small portion of the mainstream aortic flow is intercepted by the sinus ridge, or downstream corner of the sinus of Valsalva. This fluid curls back toward the ventricle to form a large eddy, or vortex, that spins within the sinus cavity. The fluid motion within similar recirculating flows is known to be unstable with an early transition to turbulence. The stability of the aortic sinus vortex was examined in the current study in an in vitro pulsatile flow rig. The geometry of the experimental test section was the same as the geometry of the natural aortic root. Different model valves, including a natural valve, were placed in the test section, and different flow conditions were studied. Point velocities were measured by hot film probes placed at two locations within the sinus vortex. The velocity waveforms and their power spectra were used to determine the stability of the sinus flow. The experimental results revealed that the aortic sinus vortex becomes turbulent under simulated exercise conditions. Turbulent intensities were highest near the sinus ridge, which is the location of the coronary ostia. Despite the transition to turbulence within the vortex, the mainstream aortic flow upstream from the valve remained laminar. The turbulence within the vortex was also associated with vibration of the valve leaflets under exercise conditions. These vibrations may be related to the systolic ejection murmurs that are heard clinically. Furthermore, the localized turbulence may explain the location of atherosclerotic lesions and dissecting aneurysms, as well as the distribution of the lesions of bacterial endocarditis. (*Circulation Research* 1990;67:448–460)**



It is the purpose of this paper to present experimental studies on the onset of turbulence within the sinus vortices. These vortices, formed within the outpocketings of the sinus of Valsalva at the base of the aorta, have been studied by numerous authors since da Vinci[1] first described them. However, the stability of these vortices has never been previously examined. The onset of turbulence in the vortices is an important phenomenon, as it may help to clarify the etiology of systolic ejection murmurs and atherosclerotic heart disease.

Before considering the stability of the vortices, however, it is important to understand the underlying flow pattern and the terminology of separated flows. Upstream from the sinus cavities there is little variation in velocity with radial position, with the exception of the thin boundary layer that travels next to the aortic wall. Within these outer laminas of the mainstream flow, the velocity changes from zero at the wall to its maximum midstream value. When this layer reaches the tip of the fully open valve leaflets, it is forced to separate from the wall to continue downstream as a free shear layer. Figure 1 illustrates the change in the velocity profile that occurs with the onset of boundary layer separation.

Of course, when the separated shear layer is intercepted by the sinus ridge, a portion of the fluid begins to curl back toward the ventricle. A spinning vortex, or eddy current, is thus formed within each sinus cavity. Each vortex spins in the direction shown schematically in Figure 1, being driven by momentum transferred across the free shear layer from the mainstream flow.

The flow within the vortex can be well ordered and laminar, or it can become turbulent, with superimposed random motion of the fluid particles. It is this transition to turbulence within the vortex that is examined in detail in this study.

*Flow in the mainstream aorta.* The systolic flow at the base of the pulmonary artery or aorta can thus be divided into an unsteady mainstream flow and the vortices that spin within the sinuses of Valsalva. The mainstream flow provides a logical starting point for the discussion of large artery hemodynamics, as the fluid mechanics of this flow are well understood.

The mainstream flow can be subdivided into both steady and oscillatory flow components. The steady component is in fact a standard problem treated in any of the fluid mechanics textbooks, such as that of

From the University of Oxford, Oxford, England.
Supported by the Rhodes Trust.
Address for correspondence: Jon A. Peacock, MD, PhD, Apt. 329N, 5225 Pooks Hill Road, Bethesda, MD 20814.
Received March 25, 1986; accepted March 30, 1990.

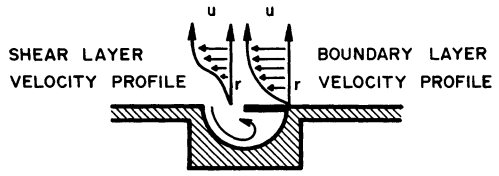


FIGURE 1. *Schematic representation of boundary layer and shear layer velocity profiles. u, velocity; r, pipe radius.*

Bennet and Myers.[2] The transition to turbulence in this component is known to occur when the steady flow Reynolds number ($Re_D=2ru_b/\nu$, where $Re_D$ is the steady flow Reynolds number based on pipe diameter, r is the pipe radius, $u_b$ is the steady flow plug [bulk] velocity, and $\nu$ is the kinematic viscosity) reaches a value greater than 2,100. (Refer to Table 1 for glossary of symbols.) For Reynolds numbers greater than 2,500, continuous turbulence that becomes more intense is observed.

The theoretical description of the mainstream oscillatory flow component was given by Womersley,[3] who developed the dimensionless frequency parameter: $\alpha=r(\omega/\nu)^{0.5}$, where $\alpha$ is the Womersley parameter and $\omega$ is the oscillatory frequency in radians per second. This parameter governs the shape of the velocity profiles. Although this solution is only valid for laminar profiles, the onset of turbulence in the unsteady mainstream flow has been extensively investigated.[4,5] These experimental studies have shown highly disturbed velocity waveforms to be the exception rather than the rule. However, instabilities can be observed in the mainstream at peak forward flow, with the disturbances persisting throughout the decelerating phase.

**TABLE 1. Glossary of Symbols**

| | |
|---|---|
| $\alpha$ | Womersley parameter$=r(\omega/\nu)^{0.5}$. |
| D | Pipe diameter. |
| E | Elastic modulus of valve material. |
| f | Frequency of piston oscillation (Hz). |
| Q | Steady volumetric flow (cc/sec). |
| r | Pipe radius. |
| Re | Steady flow Reynolds number based on pipe radius$=ru_b/\nu$. |
| $Re_D$ | Steady flow Reynolds number based on pipe diameter$=2ru_b/\nu$. |
| $Re_{peak}$ | Peak flow Reynolds number based on pipe radius$=ru_{max}/\nu$. |
| Strouhal number | $r^3/(A_1K)$, where $A_1$ is the cross-sectional area of the test section ($\pi r^2$) and K is maximum piston displacement. |
| t | Valve thickness. |
| %Turbulence | Turbulence intensity$=100(U_1-U_2)/(U_1+U_2)$. |
| u | Velocity. |
| $u_b$ | Steady flow plug (bulk) velocity$=Q/\pi r^2$. |
| $u_{max}$ | Maximum (peak) forward velocity. |
| $U_1$ | Upper bound to turbulent peak velocity. |
| $U_2$ | Lower bound to turbulent peak velocity. |
| $\nu$ | Kinematic viscosity$=\mu/\rho$, where $\mu$ is fluid viscosity and $\rho$ is fluid density. |
| $\omega$ | Frequency in radians/sec. |

*Flow in the sinus of Valsalva.* For simple two-dimensional systems, an analytical solution for the velocity field within a vortex can be obtained.[6] Unfortunately, a three-dimensional solution for the flow pattern in the sinus of Valsalva has not been obtained, even for the case of a laminar vortex. Furthermore, although the boundary layer may be laminar at separation, transition can then occur so that at reattachment the shear layer is transitional or completely turbulent. The theoretical description of this process is incompletely understood, even for a simple case such as flow past a circular cylinder.[7]

The onset of turbulence in a two-dimensional vortex, with a geometry similar to that of the sinus of Valsalva, is shown in the particle photographs of Figures 2–4. The steady mainstream flow in this case was between two parallel plates spaced 0.5 cm apart. Semicircular cavities, of 1.0-cm diameter, extended from the side of each of the plates. A metal valve leaflet extended over 75% of the cavity on the right side of the photographs, as if it were in the fully open position. No leaflet was placed over the cavity on the left side of the photographs. For the orientation shown in these figures, the mainstream flow was directed from the bottom to the top of the channel.

Figure 2 illustrates laminar vortices in both of the cavities, with Re=50. Figure 3 also illustrates laminar vortices, but with Re=150. Figure 4 illustrates turbulent vortices, which were observed at Re=1,500.

These photographs thus serve to illustrate the onset of turbulence within a separated flow. In addition, they demonstrate that the presence of a leaflet pushes the vortex into the downstream corner of the cavity. Since a theoretical description of such a vortex is impossible, the stability of the sinus vortices was studied experimentally in a rig designed to mimic flow through the semilunar valves.

## Materials and Methods

The model heart valves discussed in this section were all placed in the test rig shown schematically in Figure 5. As described elsewhere,[8] this test rig provided an oscillatory sine wave flow pulse superimposed on a steady flow. A test section that matched the geometry of the aortic and pulmonary roots was employed, with detachable model sinuses of Valsalva that were made of Plexiglas. The photograph in Figure 6 shows the test section, complete with a model valve made of latex rubber. The photograph in Figure 7 shows one of the detachable sinuses, with a wall shear probe in place near the sinus ridge.

Sketches of the pertinent geometry and dimensions of the test section are given in Figure 8. Two of the three sinuses were used for differential pressure measurements using quartz gauges (type 7251, Kist-

FIGURE 2. *Particle photograph showing steady flow laminar vortices with a Reynolds number of 50.*

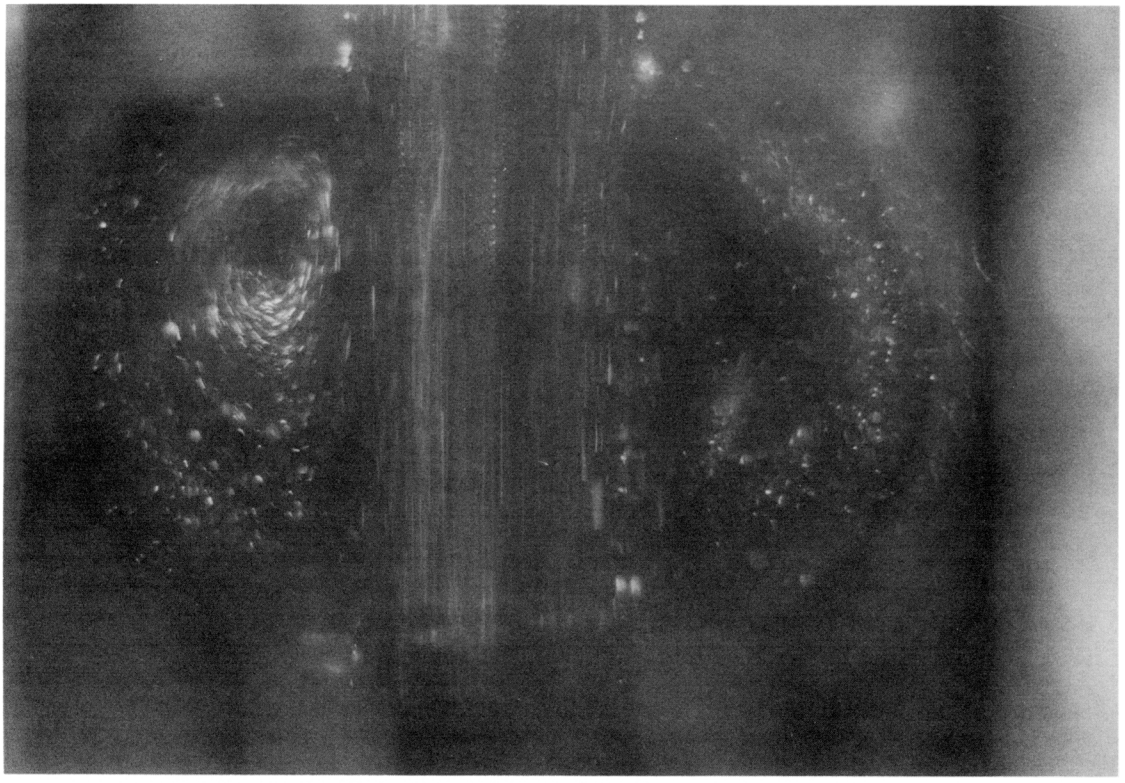

FIGURE 3. *Particle photograph showing steady flow laminar vortices with a Reynolds number of 150.*

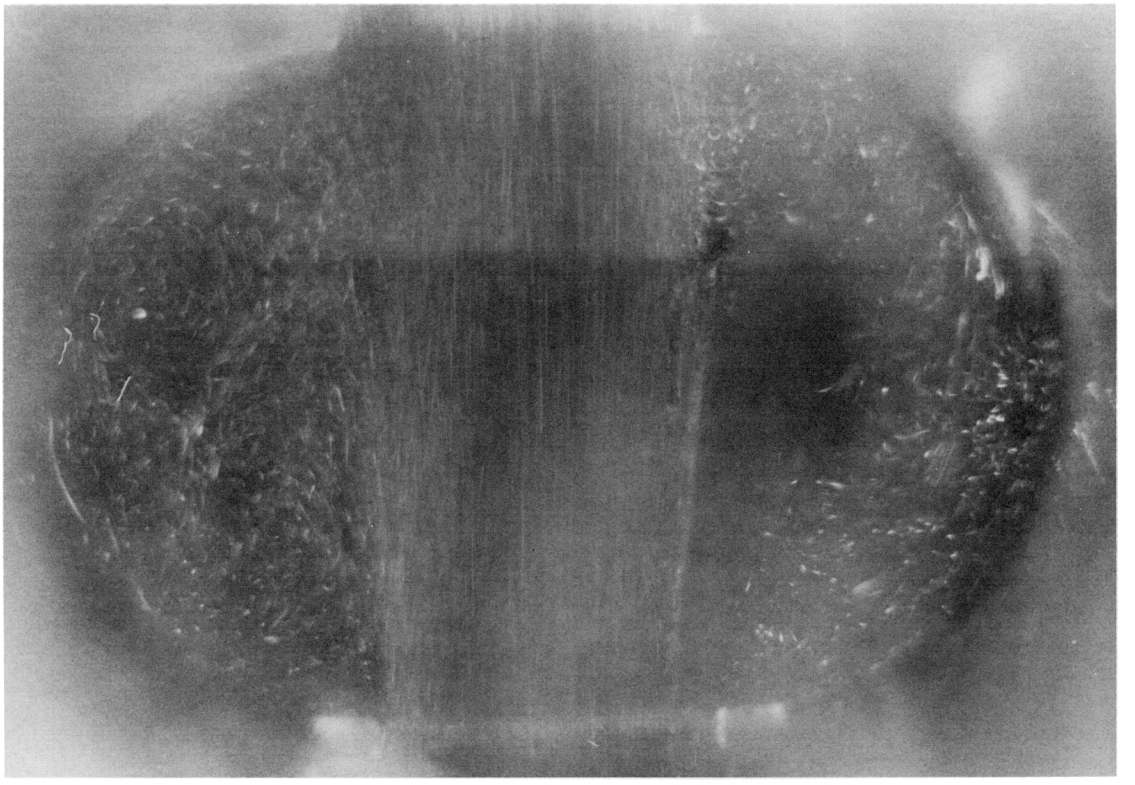

FIGURE 4. *Particle photograph showing steady flow turbulent vortices with a Reynolds number of 1,500.*



ler Instrument Corp., Amherst, N.Y.); the third sinus was used for velocity measurements with the thin film probes described by Peacock and Stairmand.[9] The sketches in Figure 8 show the location of the wall pressure taps and the location of the seals for the thin film probes. All of the pressure taps and seals located in the sinuses were placed in a midline position.

Downstream from the test section itself, a viewing piece allowed the motion of the valve cusps to be photographed at 50 frames/sec with a cine camera. Each of the thin film probes was calibrated in the mainstream flow, before being placed in its final position. Probe S3 was located at the sinus ridge after calibration, 2 mm from the sinus wall. Probe S2 was placed in a midsinus position, 2 mm from the sinus wall. Probe S1 remained in the centerline calibration position in the mainstream flow.

With all of the probes properly positioned, a steady water flow was selected by adjusting the needle valve on the test rig. The stroke of the oscillatory piston was then selected, and its frequency was increased slowly until the valve cusps were observed to close.

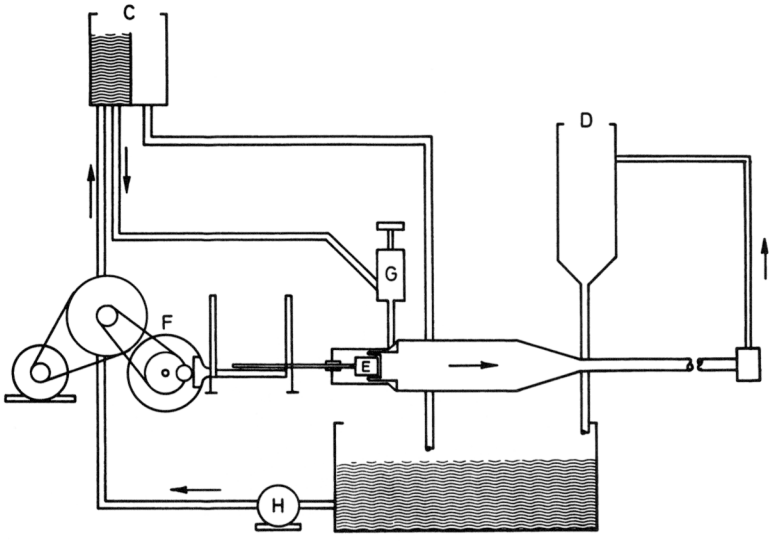


FIGURE 5. *Schematic representation of pulsatile flow test rig. C, upstream header tank; D, downstream tank; E, piston attached to shaker (F); G, steady-flow control valve; H, recirculation pump. The test section was placed in the gap between E and D. Arrows indicate direction of steady flow through the test rig.*

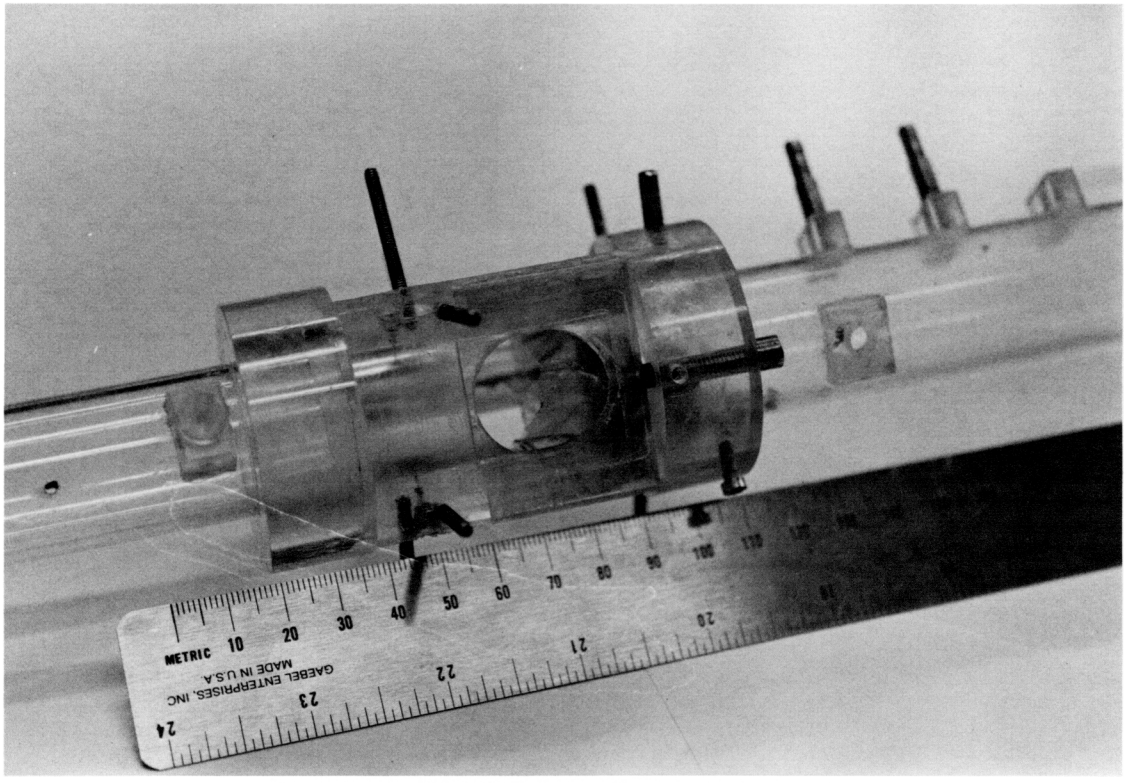


FIGURE 6. *Photograph of model valve test section.*

The mean volumetric flow was then accurately measured, using a bucket and stopwatch.

For each such set of closure conditions, dye was injected into the sinus to observe the sinus vortex, and data from the pressure and velocity probes were stored on a reel-to-reel tape machine (Ampex, London, UK). These data were later sampled for analog-to-digital conversion by an AR-11 module of a PDP-11 minicomputer (Digital Equipment Corp., London, UK). After conversion to calibrated velocities and pressures, the data for any particular set of closure conditions were displayed in the format shown in Figures 9–12.

The plot in the upper right corner in Figures 9–12 displays the signal from the velocity probe S3. The abscissa is the dimensionless cycle time; the ordinate is in centimeters per second. The next plot to the left similarly shows the signal from S2; the plot in the upper left corner shows the signal from S1. On this latter plot, the motion of the cusps as determined from the cinefilm analysis is also presented. The ordinate in this case is the percentage of the cross-sectional area between the leaflet tips that remained open. Thus, the valve is fully closed at 0% and fully open at 100%. These measurements were obtained by dividing the area between the cusp tips at a particular time by the maximum area between the cusp tips as measured at peak systole.

The final stage in the data analysis was to calculate power spectra for the three velocity probe signals. The fast fourier transform routine given in the study of Brigham[10] was used directly for this purpose. On completion of the routine, XR was the real part of the transform, and XI was the imaginary part. The transform was accurate to a maximum frequency of 1/2T, where T is the time increment between the digital samples. The power spectrum was calculated as $(XR^2+XI^2)^{0.5}$. The mean component was set to zero, and the spectra were then normalized using the maximum absolute value. The power spectra plots for each of the probes are shown beneath the corresponding velocity plots in Figures 9–12. The normalized ordinate of these plots ranges from zero to one; the abscissa is given in units of frequency (hertz).

## Results

To examine the effects of the elastic properties of the leaflet material, several different model heart valves were placed in the test rig. In Table 2, the elastic modulus and the thickness of each of these leaflet materials are listed. The thickness was measured by a micrometer; the elastic modulus was measured with an Instron apparatus (Instron Corp., Canton, Mass.) as in Clark[11] and Broom.[12]

For each of these valves, data from the pressure and velocity transducers were collected for a wide range of closure conditions. Both resting states and exercise conditions (higher stroke volumes and/or higher heart rates) were studied. The closing efficiency of the various valves and other dependent dimensionless groups was correlated, as previously described in detail by the author.[8] Only the salient features of the transition to turbulence within the sinus vortex are presented here.

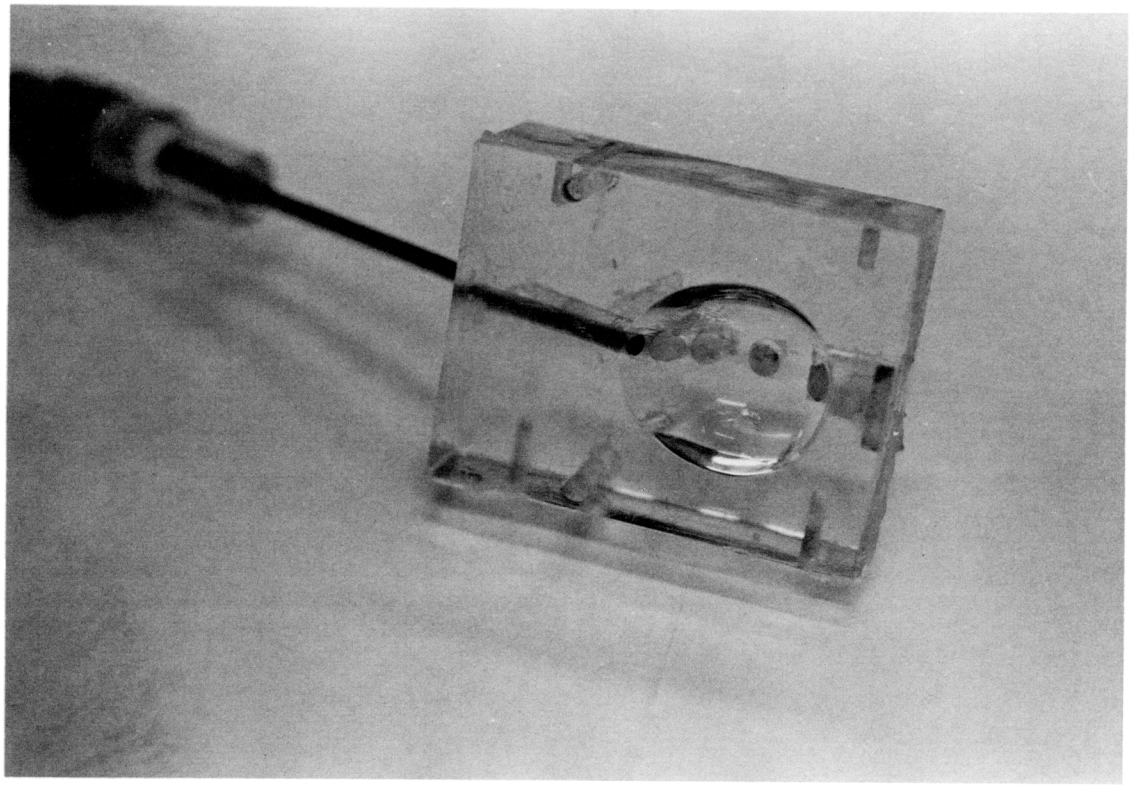

FIGURE 7. *Photograph of model sinus of Valsalva. A wall shear probe is in place near the sinus ridge.*

In the first instance, it is useful to consider the flow patterns present without any valve in the test rig. Data for both resting and exercise conditions without a valve are shown in Figures 9 and 10, respectively. For the resting condition shown in Figure 9, there are few peaks superimposed on either the mainstream (S1) or sinus waveforms (S2 and S3). The power spectra are also consistent with a completely laminar flow, as all of the energy is concentrated at the frequency of the underlying pulsatile flow.

For the exercise condition shown in Figure 10, however, multiple velocity spikes are seen superimposed on the underlying sinus flow. The S2 and S3 power spectra also reveal the presence of higher frequency components consistent with a turbulent vortex. The mainstream flow upstream from the valve (S1) still appears to be laminar, despite the presence of a higher peak flow.

Similar observations were also made when valves were placed in the test rig. Of course, the natural (bovine) valve provided the most accurate physiological information. Data for both resting and exercise conditions for this valve are shown in Figures 11 and 12, respectively. In terms of turbulence, a feature of importance in the S2 waveform in Figure 11 is that there are two superimposed velocity peaks. Similar peaks were seen under resting conditions in other experiments. Such peaks may be due to movement of the laminar vortex core during the cycle, as described by Bellhouse and Talbot.[13] Alternatively, they could

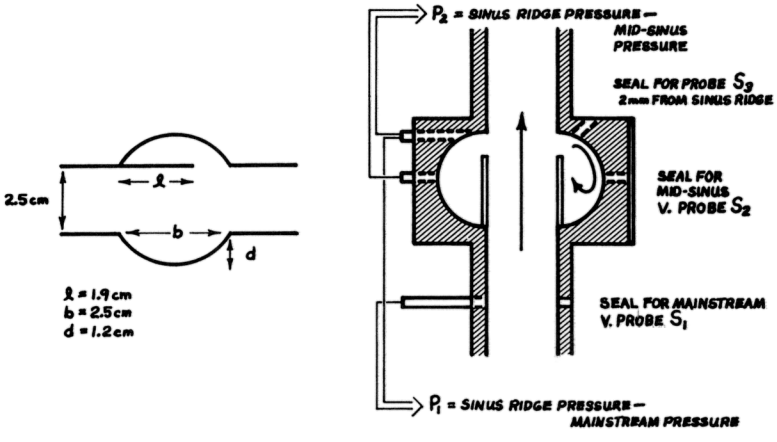


FIGURE 8. *Schematic representation showing dimensions of the test section* (left panel) *and location of wall pressure taps ($P_1$ and $P_2$) and seals for the velocity probes* (right panel). *Arrows in right panel indicate direction of flow.*

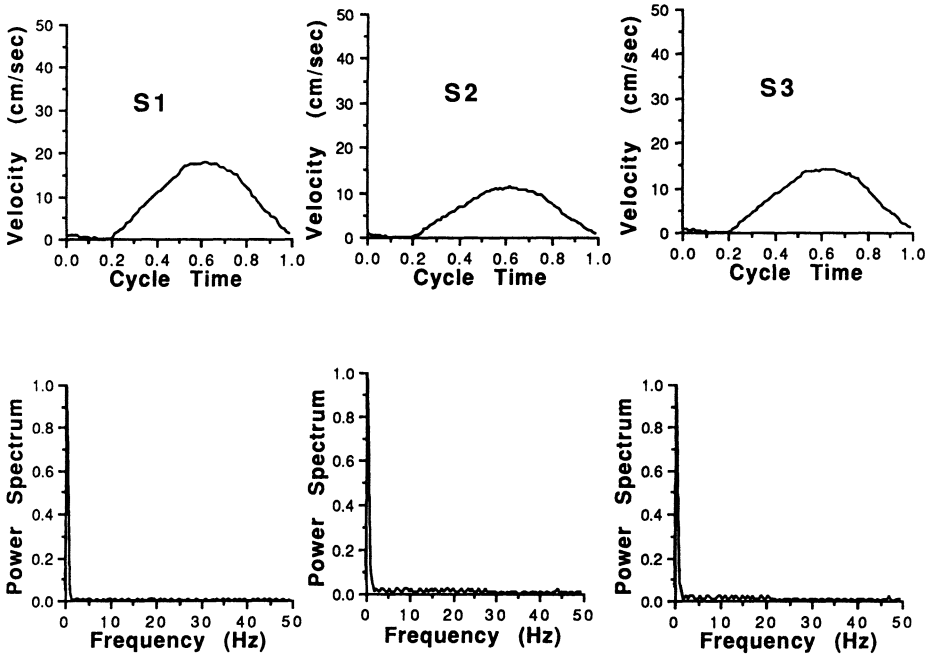


FIGURE 9. *Plots showing a simulated resting condition without a valve.* Top panels: *Signals from velocity probes S1, S2, and S3.* Bottom panels: *Power spectra for the three velocity probe signals. Re=817, $Re_{peak}$=1,763, $\alpha^2$=607, and f=0.49 Hz, where Re is the steady flow Reynolds number, $Re_{peak}$ is the peak Re, $\alpha$ is the Womersley parameter, and f is the frequency of piston oscillation.*

represent a transitional velocity pattern. A precise interpretation of these peaks is difficult.

In the case of the peaks superimposed on the output from probe S3 in Figure 11, the interpretation is simpler. Multiple velocity spikes such as these could not be due to the movement of a laminar vortex but instead suggest a transition to turbulence within the separated flow. This interpretation is also supported by the power spectrum for S3, which shows a broad spectrum of high-frequency components. In contrast, the spectrum for probe S2 contains significant components only near 2 Hz, due to the two peaks previously described.

Under exercise conditions, high-frequency components were found in the output of both sinus probes. This is shown in Figure 12, where the output of probes S2 and S3 appears completely turbulent. Only the mainstream signal recorded by S1 still appears laminar despite the higher peak flow.

It is important to note that when the natural valve cusps were fully open under these same exercise conditions, they were observed to vibrate with an

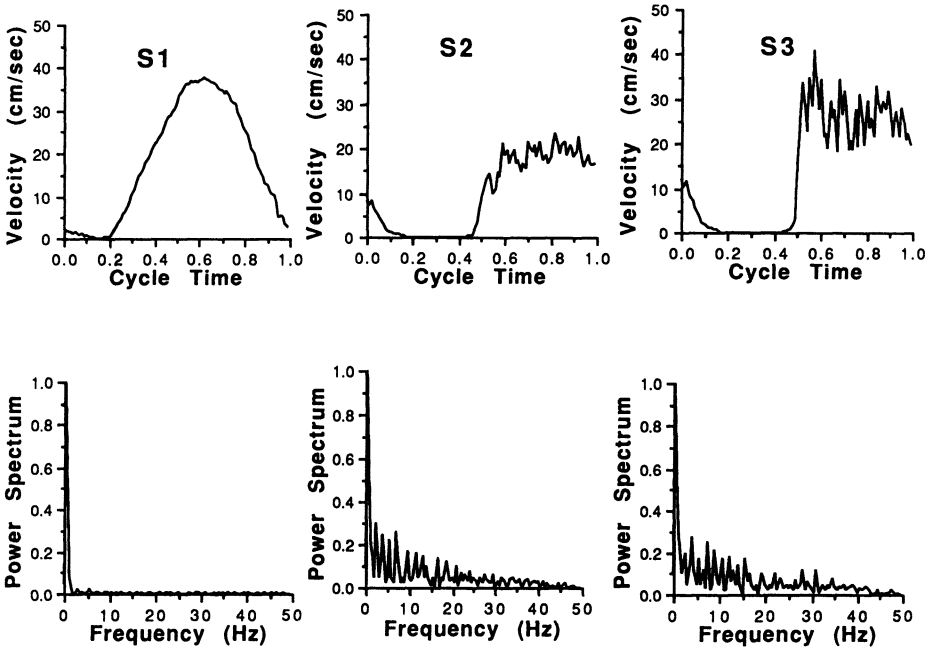


FIGURE 10. *Plots showing a simulated exercise condition without a valve.* Top panels: *Signals from velocity probes S1, S2, and S3.* Bottom panels: *Power spectra for the three velocity probe signals. Re=1,570, $Re_{peak}$= 5,039, $\alpha^2$=605, and f=0.48 Hz, where Re is the steady flow Reynolds number, $Re_{peak}$ is the peak Re, $\alpha$ is the Womersley parameter, and f is the frequency of piston oscillation.*

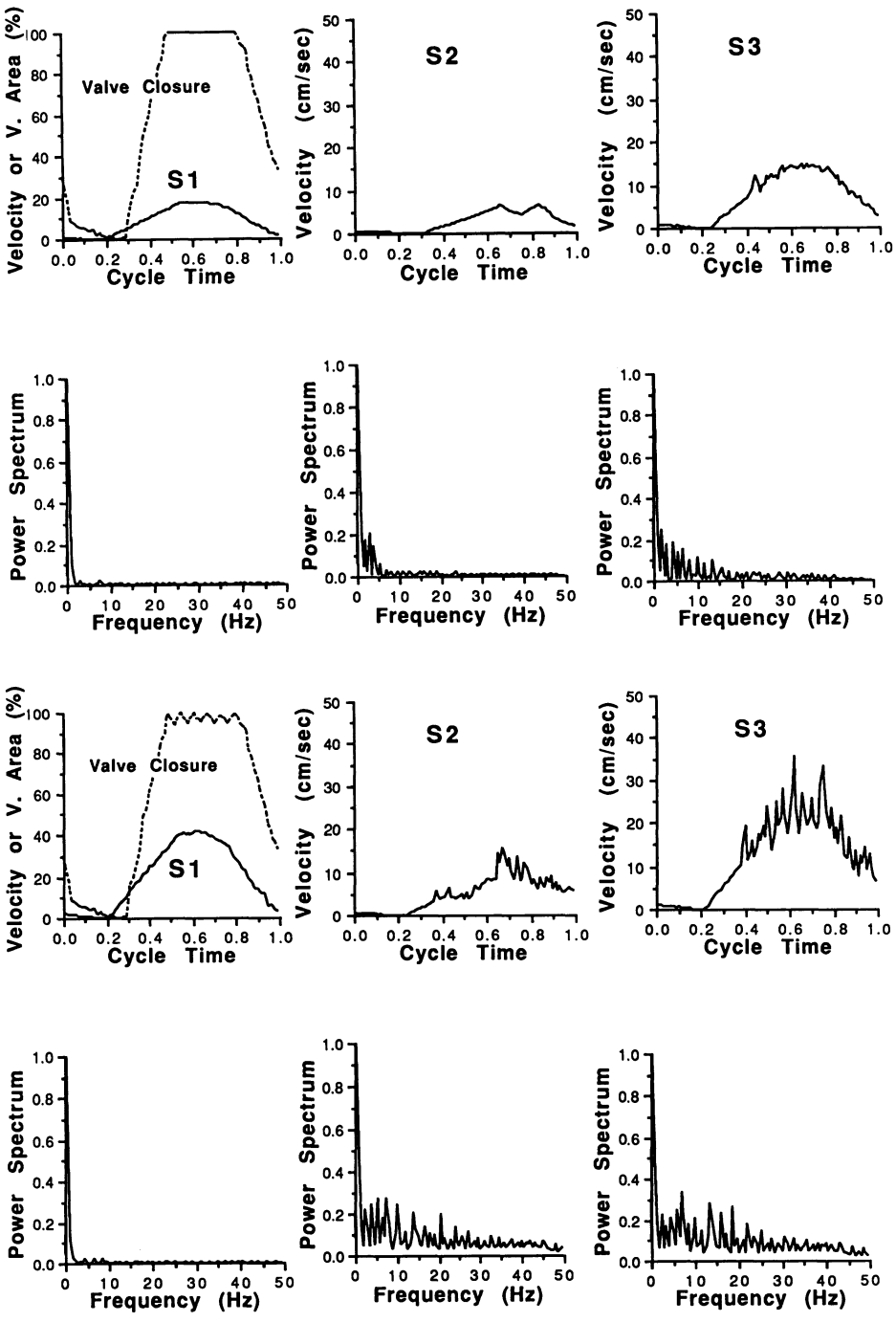


FIGURE 11. *Plots showing a simulated resting condition with a natural valve.* Top panels: *Signals from velocity probes S1, S2, and S3.* Bottom panels: *Power spectra for the three velocity probe signals. Re=495, $Re_{peak}$=1,293, $\alpha^2$=315, and f=0.29 Hz, where Re is the steady flow Reynolds number, $Re_{peak}$ is the peak Re, $\alpha$ is the Womersley parameter, and f is the frequency of piston oscillation.*




FIGURE 12. *Plots showing a simulated exercise condition with a natural valve.* Top panels: *Signals from velocity probes S1, S2, and S3.* Bottom panels: *Power spectra for the three velocity probe signals. Re=2,787, $Re_{peak}$=5,769, $\alpha^2$=587, and f=0.54 Hz, where Re is the steady flow Reynolds number, $Re_{peak}$ is the peak Re, $\alpha$ is the Womersley parameter, and f is the frequency of piston oscillation.*

amplitude of approximately 2 mm and a frequency of approximately 30 Hz. These values are only approximate, since the cinefilm itself was taken at only 50 frames/sec. The fluttering is shown during systole on the leaflet motion plot in Figure 12.

These representative samples have thus demonstrated that it was possible to qualitatively divide the S2 and S3 signals into laminar, transitional, and fully turbulent waveforms as outlined by other authors.[5,14] The power spectra of the turbulent waveforms were very useful in distinguishing between laminar and turbulent flow conditions. As expected in a turbulent flow,[14] the observed spectra were continuous with a random energy distribution. The energy distribution also decreased smoothly with increasing frequency.

To quantify the results for the fully turbulent waveforms, the intensity of the turbulence in these signals was defined as in Bellhouse and Talbot[13]:

$$\%\text{Turbulence}=\frac{100(U_1-U_2)/2}{(U_1+U_2)/2}=100\frac{(U_1-U_2)}{(U_1+U_2)}$$

**TABLE 2. Material Properties of the Model Valves**

| Material | E ($N/m^2$) | t(mm) |
|---|---|---|
| Biomer | $5.30\times10^6$ | 0.193 |
| PTFE | $2.75\times10^7$ | 0.033 |
| Latex | $6.26\times10^5$ | 0.069 |
| Natural | $1.95\times10^4$ | 0.300 |

E, elastic modulus of valve material; t, valve thickness; PTFE, polytetrafluoroethylene.

where $U_1$ is the upper bound to the peak forward velocity and $U_2$ is the lower bound to the peak forward velocity.

Tables 3–9 list the results for the various valve materials tested. A laminar or transitional condition of the waveform is indicated as such, and the intensity of any fully turbulent waveforms is given directly. The length of the valve leaflets in each case was 1.9 cm, unless otherwise specified.

## Discussion

### *Transition to Turbulence Within the Mainstream*

As previously discussed, transition to turbulence within the core of the large arteries has been studied by Schultz et al[4] and Nerem and Seed.[5] It is of interest to compare their results with the output of probe S1, which was located within the mainstream flow in the current experiments.

In both of the above studies, disturbances were noted in the mainstream flow for very high peak velocities. Such disturbances were felt to be generated within the boundary layer next to the aortic wall or convected downstream from the ventricle itself. Assuming that the disturbances were generated within the boundary layer, Nerem and Seed[5] derived an expression for the critical peak Reynolds number ($Re_{D_{(critical)}}=u_{max}D/\nu$, where $u_{max}$ is the maximum [peak] forward velocity) from boundary layer stability theory. The form of the equation was

$$Re_{D_{(critical)}}=\text{constant}\times\alpha \quad (1)$$

where the theoretical value of the constant ranged from 250 to 1,000.

Equation 1 demonstrates that a higher peak Reynolds number is required for transition to occur if $\alpha$ is increased. This is reasonable, as increasing $\alpha$ decreases the time available for the amplification of disturbances. In their in vivo measurements, Nerem and Seed[5] found that the constant was 250 in the descending aorta but only 150 in the ascending aorta. They attributed this difference to disturbances from the aortic valve leaflets.

These authors displayed typical examples of undisturbed (laminar), disturbed (transitional), and highly disturbed (turbulent) pulsatile waveforms. In the

**TABLE 3. Sinus Turbulence Data Without a Valve in the Test Section**

| Re | $Re_{peak}$ | $\alpha^2$ | Turbulence intensity S2 | Turbulence intensity S3 |
|---|---|---|---|---|
| 828 | 1,279 | 292 | L | L |
| 817 | 1,763 | 607 | L | L |
| 822 | 1,778 | 290 | L | TR |
| 1,576 | 2,543 | 291 | L | T |
| 817 | 2,746 | 1,232 | ... | ... |
| 822 | 2,824 | 606 | ... | ... |
| 1,570 | 3,229 | 290 | TR | TR |
| 1,549 | 3,557 | 606 | TR | TR |
| 822 | 3,806 | 480 | ... | ... |
| 1,517 | 3,900 | 291 | TR | 7.7 |
| 3,661 | 4,711 | 606 | TR | TR |
| 1,570 | 5,039 | 605 | TR | 12.8 |
| 1,507 | 5,600 | 1,237 | TR | TR |
| 3,703 | 5,632 | 606 | TR | 14.3 |
| 3,608 | 5,756 | 1,232 | 28.6 | 33.3 |
| 3,650 | 7,301 | 606 | 16.3 | 23.1 |
| 3,618 | 8,596 | 609 | 7.3 | 20.0 |
| 3,119 | 10,624 | 1,250 | 22.0 | 30.0 |

Re, steady flow Reynolds number; $Re_{peak}$, peak Re; S2 and S3, velocity probes; L, laminar condition of the waveform; TR, transitional condition of the waveform. No valve fluttering was observed.

**TABLE 4. Sinus Turbulence Data for 0.193-mm Biomer Valve**

| Re | $Re_{peak}$ | $\alpha^2$ | Turbulence intensity S2 | Turbulence intensity S3 |
|---|---|---|---|---|
| 520 | 4,274 | 1,094 | L | TR |
| 562 | 4,586 | 648 | L | TR |
| 1,586 | 6,287 | 1,370 | L | TR |
| 1,645 | 6,614 | 802 | L | TR |
| 1,724 | 7,004 | 407 | L | TR |
| 3,539 | 9,344 | 938 | L | TR |
| 3,576 | 9,937 | 649 | L | TR |
| 3,586 | 10,156 | 507 | L | TR |

Re, steady flow Reynolds number; $Re_{peak}$, peak Re; $\alpha$, Womersley parameter; S2 and S3, velocity probes; L, laminar condition of the waveform; TR, transitional condition of the waveform. No valve fluttering was observed.

**TABLE 5. Sinus Turbulence Data for Bovine (Natural) Valve**

| Re | $Re_{peak}$ | $\alpha^2$ | Turbulence intensity S2 | Turbulence intensity S3 | Cusp fluttering Amplitude (mm) | Cusp fluttering Frequency (Hz) |
|---|---|---|---|---|---|---|
| 495 | 1,293 | 315 | L | TR | ... | ... |
| 769 | 1,904 | 225 | L | 14.3 | 0.5 | 15 |
| 1,839 | 3,906 | 812 | L | 25.2 | ... | ... |
| 1,764 | 3,906 | 213 | TR | 25.7 | 1.0 | 20 |
| 1,768 | 4,003 | 440 | TR | 37.5 | 1.0 | 20 |
| 2,811 | 5,226 | 952 | TR | 38.5 | 1.5 | 25 |
| 2,787 | 5,769 | 587 | TR | 34.7 | 2.0 | 30 |
| 2,839 | 6,033 | 316 | 18.2 | 41.2 | 2.0 | 30 |

Re, steady flow Reynolds number; $Re_{peak}$, peak Re; $\alpha$, Womersley parameter; S2 and S3, velocity probes; L, laminar condition of the waveform; TR, transitional condition of the waveform.

latter case, high-frequency velocity components were found superimposed on the pulsatile mainstream flow. These components were observed during peak systole and the subsequent decelerating phase of the flow, when inflection points appeared in the mainstream velocity profiles. Power spectra revealed frequency components above those of the underlying pulsatile flow.

As has been previously mentioned, the output of probe S1 appeared laminar throughout all the pulsatile experiments conducted in the test rig. This was confirmed by the lack of high-frequency components in the power spectra for this probe and is consistent with Equation 1 if the constant is assumed greater than or equal to 750. Since S1 was located upstream from the valve leaflets, it is not surprising that the value of the constant is higher than that found by Nerem and Seed.[5]

To confirm that the turbulence detected by probes S2 and S3 was not due to the invasive nature of the measurements, preliminary studies with a wall shear probe were also carried out.[8] These measurements, made with hot films mounted flush with the aortic and sinus walls, did confirm the accuracy of the measurements made by the needle probes. Furthermore, pulsatile mainstream turbulence was detected with a wall shear probe at $Re_{D(critical)}=20,350$ and $\alpha=27$. This is also consistent with a value of 750 for the mainstream constant in the current experimental rig.

*Transition to Turbulence Within the Vortex*

Although the mainstream probe S1 remained laminar throughout the experiments, probes S2 and S3 displayed evidence of superimposed turbulence under simulated exercise conditions. Other authors have studied the onset of turbulence in separated flows, and their work will be briefly reviewed here before discussing the S2 and S3 data.

Gillani and Swanson,[15] in their theoretical study of the aortic sinus vortex, predicted that instabilities would appear within the vortex at velocities only slightly higher than those in their study. Since their study dealt only with physiological resting conditions, their prediction is clearly borne out by the present experimental work.

Other studies relating directly to the sinus of Valsalva are unfortunately not available, but other authors[16,17] have studied similar geometries in experimental rigs. Feuerstein et al[16] studied the vortex produced by an abrupt expansion in a circular tube. An instability was first noted within the vortex near the reattachment point. This instability was periodic in nature (spectra with well-defined frequency peaks) and was observed at a Reynolds number of 1,090. As the Reynolds number was further increased, the region of instability moved back toward the separation point. Furthermore, the turbulence became completely random in nature.

Back and Roschke[17] obtained similar results for a similar steady flow and geometry, except that transition occurred at a Reynolds number (based on the upstream tube diameter) of only 250. Their upstream velocity profile was blunt, in contrast to the parabolic profile in the work by Feuerstein et al.[16] This may explain the different results, as the velocity in the shear layer would be lower in the latter case. The most important point, of course, is that turbulence was observed in the vortices of both studies before its onset in the mainstream flow.

The transitional state, which first signals the onset of turbulence in the free shear layer, has been extensively studied by Rockwell and Naudascher[18] and Rockwell and Knisely.[19] A complex feedback mechanism (from the downstream cavity wall back to the separation point) is believed to be responsible for the onset of the instabilities. The theoretical model is as yet incomplete, in that only the shear layer (and not the entire cavity flow) is considered.

Although the previous authors dealt only with steady flows, Stephanoff[20] studied the transition to turbulence in the hollows of the Bellhouse model oxygenator. The mainstream flow in this case was a pulsatile sine wave with a small superimposed steady component. Stephanoff found the onset of vortex instabilities for this geometry at a peak Reynolds number (based on half the minimum channel height)

**TABLE 6. Sinus Turbulence Data for 0.033-mm PTFE Valve**

| Re | $Re_{peak}$ | $\alpha^2$ | Turbulence intensity S2 | Turbulence intensity S3 |
|---|---|---|---|---|
| 962 | 2,474 | 224 | L | ... |
| 1,401 | 3,336 | 762 | L | TR |
| 1,518 | 3,795 | 251 | L | 7.7 |
| 2,023 | 4,754 | 404 | L | TR |
| 2,763 | 5,365 | 1,027 | ... | TR |
| 2,424 | 5,713 | 338 | L | 12.0 |
| 2,877 | 6,311 | 506 | L | 14.3 |
| 2,839 | 6,436 | 369 | L | 25.0 |

Re, steady flow Reynolds number; $Re_{peak}$, peak Re; $\alpha$, Womersley parameter; S2 and S3, velocity probes; L, laminar condition of the waveform; TR, transitional condition of the waveform. No valve fluttering was observed.

**TABLE 7. Sinus Turbulence Data for 0.069-mm Latex Rubber Valve**

| Re | $Re_{peak}$ | $\alpha^2$ | Turbulence intensity S2 | Turbulence intensity S3 | Cusp fluttering Amplitude (mm) | Cusp fluttering Frequency (Hz) |
|---|---|---|---|---|---|---|
| 505 | 1,307 | 303 | L | L | ... | ... |
| 585 | 1,432 | 191 | L | L | ... | ... |
| 1,594 | 3,572 | 745 | L | TR | ... | ... |
| 1,721 | 3,850 | 483 | L | TR | ... | ... |
| 2,023 | 4,434 | 247 | L | TR | 0.5 | 20 |
| 2,877 | 5,560 | 1,008 | L | 11.0 | 1.0 | 20 |
| 2,905 | 5,935 | 686 | L | 33.0 | 1.5 | 25 |
| 2,924 | 6,227 | 338 | L | 33.0 | 1.5 | 25 |

Re, steady flow Reynolds number; $Re_{peak}$, peak Re; $\alpha$, Womersley parameter; S2 and S3, velocity probes; L, laminar condition of the waveform; TR, transitional condition of the waveform.

**TABLE 8. Sinus Turbulence Data for 0.069-mm Latex Rubber Valve (Leaflet Length=2.4 cm)**

| Re | $Re_{peak}$ | $\alpha^2$ | Turbulence intensity S2 | Turbulence intensity S3 | Cusp fluttering Amplitude (mm) | Cusp fluttering Frequency (Hz) |
|---|---|---|---|---|---|---|
| 490 | 1,362 | 292 | L | L | ... | ... |
| 1,481 | 3,378 | 337 | L | L | ... | ... |
| 1,707 | 3,795 | 703 | L | L | ... | ... |
| 1,825 | 4,101 | 223 | L | L | ... | ... |
| 2,249 | 4,990 | 270 | L | L | ... | ... |
| 2,886 | 6,088 | 315 | L | L | 1.0 | 20 |
| 2,928 | 6,088 | 562 | L | ... | 1.0 | 20 |

Re, steady flow Reynolds number; $Re_{peak}$, peak Re; $\alpha$, Womersley parameter; S2 and S3, velocity probes; L, laminar condition of the waveform; TR, transitional condition of the waveform.

of only 100. The transitional state was not characterized by a dominant disturbance frequency (as in steady cavity flows) but was more random in nature.

Transition to turbulence within separated flows has thus been studied in detail by several other authors,[16–20] although not in a rig designed to mimic flow through the sinus of Valsalva. The turbulence detected within the sinus flow in the current test rig is therefore of considerable interest.

The data in Tables 3–9 clearly indicate that the sinus vortex (S2, S3) was unstable even though the mainstream (S1) remained laminar. In retrospect, this is not too surprising. Any separated shear layer has an inflected velocity profile, which makes it inherently more unstable. This is shown schematically in Figure 1 for the case of a steady flow past an open valve cusp. The boundary layer profile upstream from the valve is parabolic in shape, with $u=0$ at the wall and $u=u_{max}$ at the center line. When the boundary layer separates from the tip of the leaflet, however, the profile changes to that of a free shear layer. The presence of an inflection point within this profile (where $\partial^2u/\partial r^2=0$) is known to lower the turbulence threshold.[21] For the case of the unsteady vortex within the sinus of Valsalva, the shear layer would therefore be unstable throughout systole.[8] The mainstream profiles, however, would only exhibit inflections during the decelerating phase of the flow.[5]

**TABLE 9. Sinus Turbulence Data for 0.069-mm Latex Valve (Leaflet Length=1.5 cm)**

| Re | $Re_{peak}$ | $\alpha^2$ | Turbulence intensity S2 | Turbulence intensity S3 | Cusp fluttering Amplitude (mm) | Cusp fluttering Frequency (Hz) |
|---|---|---|---|---|---|---|
| 481 | 1,515 | 349 | L | L | ... | ... |
| 1,118 | 2,724 | 545 | L | TR | ... | ... |
| 1,490 | 3,531 | 362 | L | 14.3 | ... | ... |
| 1,688 | 3,739 | 692 | TR | TR | ... | ... |
| 2,160 | 4,754 | 461 | L | 33.3 | 0.5 | 20 |
| 2,297 | 5,129 | 279 | TR | 41.7 | 1.0 | 25 |
| 2,862 | 5,518 | 899 | TR | 38.5 | 1.0 | 25 |
| 2,910 | 6,005 | 551 | TR | 38.5 | 1.5 | 30 |
| 2,947 | 6,366 | 338 | 16.7 | 63.0 | 1.5 | 30 |

Re, steady flow Reynolds number; $Re_{peak}$, peak Re; $\alpha$, Womersley parameter; S2 and S3, velocity probes; L, laminar condition of the waveform; TR, transitional condition of the waveform.

A major physiological consequence of this transition to turbulence within the shear layer was that it was associated with fluttering of the valve cusps. As seen in Tables 3–9, the fluttering of the compliant leaflets was linked to the development of a fully turbulent sinus vortex. As might be expected, the stiffer valves did not flutter, despite the presence of a turbulent vortex.

The amplitude of the fluttering was in fact greatest with the natural leaflet. This leaflet had the lowest elastic modulus and was also thinner near the leaflet tips.[22] Both of these factors would act to decrease the overall rigidity of this particular material and thereby lead to increased fluttering.

Many other authors[23,24] have noted fluttering of the valve cusps, although it has never been linked to a turbulent vortex. For example, Rainer et al[23] observed fluttering of valve cusps placed in accelerated fatigue rigs. Thickened cusps composed of pericardial tissue were not observed to vibrate, nor did stiffer materials. Likewise, replacing the standard water test fluid with glycerol eliminated the fluttering. This is consistent with the data in Tables 3–9, since increasing the fluid viscosity decreases the magnitude of $\alpha^2$, Re, and $Re_{peak}$.

Bellhouse[24] also observed fluttering of the valve leaflets and noted that it increased in amplitude when the gap from the tip of the leaflet to the sinus ridge was increased. Since increasing this gap will decrease the stability of the cavity shear layer,[25] this is also consistent with the explanation of the fluttering presented in this section. The data in Tables 3, 7, 8, and 9 also demonstrate that transition is delayed when this gap is decreased in length. As suggested in Figures 2–4, decreasing this gap also pushes the vortex downstream within the sinus. This explains the smaller S2 velocities in Figures 11 and 12, as compared with Figures 9 and 10.

### *Clinical Implications*

*The fatigue life of the heart valves.* The natural heart valves have a remarkable 4 billion–cycle fatigue life under normal conditions. Various factors may alter their fatigue life, especially in the case of artificial valves. For example, porcine replacement valves fatigue after only 7 years.[26] Although the decreased fatigue life of the porcine valves may be related to an immune response,[27] it is important to consider the effect of the fluttering described in this paper.

Fluttering as a possible cause of leaflet fatigue has been briefly discussed by Rainer et al.[23] The severe fraying of the leaflet-free edges, as shown in Clark and Swanson,[28] was also probably caused by the fluttering of the valve tips that these authors

observed in their accelerated fatigue rig. Stein and Sabbah[29] also described jagged edges at the free margins of two degenerated porcine valves.

A porcine valve was briefly studied in the current test rig as described elsewhere.[8] Since the valve was made with the cusps in the fully closed position, it was stenotic and fluttered even under resting conditions. This constant fluttering would probably lead to increased fraying of the leaflet tips and could thereby decrease the fatigue life of the valve. Any damage due to the vibrations would certainly not be repaired, as no healing could occur within the dead leaflet tissues.

*Heart murmurs.* The valve vibrations observed during peak systole for the natural and latex leaflets are probably related not only to the fatigue life of the valves but also to the systolic ejection murmurs that are heard over the aortic and pulmonary areas. There are several indications that this is the case.

First of all, the frequency of the vibrations is the correct order of magnitude. If converted to a Strouhal number,[8] the frequency of the oscillations in blood would be of order 100 Hz. This is the order of magnitude of the sound frequencies measured at peak systole by Freis and Heath.[30] Furthermore, valve fluttering with an amplitude of 0.6 mm and a frequency of 100 Hz was noted in the in vivo experiments of Van Steenhoven et al.[31]

Second, the fact that the vibrations were not seen at rest but appeared under exercise conditions is consistent with the so-called flow murmurs heard in exercise states and other high-output states, such as pregnancy.[32] Anemia, which reduces the blood viscosity, also causes such a systolic ejection murmur. This is consistent with the current results, since $\alpha^2$, Re, and $\mathrm{Re}_{\mathrm{peak}}$ are all increased by decreasing $\nu$.

Of course, systolic ejection murmurs are also heard with severely calcified and stenotic valves. In this case, the decreased cross-sectional area will greatly increase the velocity through the valve orifice. A turbulent jet will be formed downstream from the leaflets, which may not flutter if they are severely calcified. However, the same shear layer instabilities will be present near the tip of the leaflet, and it is probably this oscillating pressure field that ultimately causes the ejection murmur itself. Indeed, the actual vibration of the leaflets may contribute more to the so-called musical component of the murmur of aortic stenosis.[33]

Other authors[29,34] have also suggested that valve vibrations are related to systolic ejection murmurs. Ratshin et al[34] observed vibrations of homograft aortic valves in twenty patients on echocardiograms. The vibrations were noted at peak systole and were associated with a systolic ejection murmur. Simultaneous phonocardiograms demonstrated that the amplitude of the leaflet vibration was proportional to the intensity of the systolic murmur. In three patients without the murmur, no vibration of the leaflets was noted.

*Pathological conditions.* The results presented in this paper also offer important clues to the understanding of a variety of pathological conditions affecting the heart. These conditions include atherosclerosis, dissecting aneurysms, and infective endocarditis.

The distribution of atherosclerotic lesions has been previously linked to the location of branch points in the large arteries, and there are many theories as to the etiology of the lesions. One of the major fluid mechanical theories was developed by Fry,[35] who postulated that local regions of high shear rates were responsible for increased cholesterol transfer and hence the lesions of atherosclerosis.

Based on the preliminary wall shear stress measurements previously reported[8] (using the probe shown in Figure 7), it is clear that the critical value for the wall shear stress determined by Fry[35] will be approached. In fact, when turbulent exercise conditions were studied, this value was exceeded in the area of reattachment at the coronary ostia. It is here that the turbulent intensities were greatest and here that the highest shear stresses in the cavity were found. Of course, it is also here at the sinus ridge and coronary ostia that the lesions of atherosclerosis are most commonly located.[36]

Such an increased wall shear stress could not only increase the mass transfer of cholesterol (causing atherosclerosis) but could also shear intimal cells from the vessel wall. Thus, dissecting aortic aneurysms could be the result of localized shear layer turbulence. In this regard, it is important to note that ascending aneurysms do in fact begin at the coronary ostia.

A final pathological condition that may be affected by localized turbulence is infective endocarditis. The characteristic distribution of bacterial colonies in infective endocarditis has been discussed in detail by Weinstein and Schlesinger.[37] For the aortic and pulmonary valves, the lesions usually form on the ventricular surface of the cusps (near the separation point at the cusp tips). Lesions associated with ventricular septal defects form near the stagnation point of the impacting jet, as well as around the downstream side of the orifice itself. The ultimate reason for these observations has remained unclear. In view of the results presented in this paper, an early transition to turbulence in these areas may damage the endothelium and lead to colony formation at these sites.

## Acknowledgments

The author would like to thank Dr. B.J. Bellhouse for the opportunity to perform the research described in this paper. The technical support of his medical engineering group is also gratefully acknowledged. Dr. I.J. Sobey provided many useful suggestions, which were instrumental in the completion of this work.

## References

1. da Vinci, Leonardo: *Quaderni d'Anatomica II.* 1513, p 9
2. Bennet CO, Myers JE: *Momentum, Heat, and Mass Transfer.* New York, McGraw-Hill Book Co, 1974, pp 36–42
3. Womersley JR: Method for the calculation of velocity, rate of flow and viscous drag in arteries when the pressure gradient is known. *J Physiol* (Lond) 1955;127:553–563

4. Schultz DL, Tunstall-Pedoe DS, Lee G, Gunning AJ, Bellhouse BJ: Velocity distribution and transition in the arterial system, in *Ciba Foundation Symposium on Circulatory and Respiratory Mass Transport,* London, July 16–18, 1968, pp 172–199
5. Nerem RM, Seed WA: An in vitro study of aortic flow disturbances. *Cardiovasc Res* 1972;6:1–14
6. Williams JC: Incompressible boundary-layer separation. *Annu Rev Fluid Mech* 1977;9:113–144
7. Kline SJ, Morkovin MV, Sovran G, Cockrell DJ (eds): *Proceedings Comp. Turbul. Boundary Layers,* Palo Alto, Calif, Stanford University, 1968, vol 1
8. Peacock JA: Heart valve haemodynamics (thesis). Oxford, England, University of Oxford, 1986
9. Peacock JA, Stairmand JW: Film gauge calibration in oscillatory pipe flow. *J Phys E Sci Instr* 1983;16:571–576
10. Brigham EO: *The Fast Fourier Transform.* Englewood Cliffs, NJ, Prentice-Hall, Inc, 1974, pp 23–67
11. Clark RE: Stress-strain characteristics of fresh and frozen human aortic and mitral leaflets and chordae tendineae. *J Thorac Cardiovasc Surg* 1973;66:202–208
12. Broom ND: The stress strain and fatigue behaviour of glutaraldehyde preserved heart-valve tissue. *J Biomech* 1977; 10:707–724
13. Bellhouse BJ, Talbot L: The fluid mechanics of the aortic valve. *J Fluid Mech* 1969;35:721–735
14. Sabbah HN, Stein PD: Turbulent blood flow in humans: Its primary role in the production of ejection murmurs. *Circ Res* 1976;38:513–525
15. Gillani NV, Swanson WM: Time-dependent laminar incompressible flow through a spherical cavity. *J Fluid Mech* 1976; 78(suppl 1):99–127
16. Feuerstein I, Pike G, Round G: Flow in an abrupt expansion as a model for biological mass-transfer experiments. *J Biomech* 1975;8:41–51
17. Back LH, Roschke EJ: Shear-layer flow regimes and wake instabilities and reattachment lengths downstream of an abrupt circular channel expansion. *J Appl Mechanics (ASME)* 1972;72:2–15
18. Rockwell D, Naudascher E: Review: Self-sustaining oscillations of flow past cavities. *J Fluids Eng Trans ASME* 1978; 100:152–165
19. Rockwell D, Knisely C: Organized nature of flow impingement upon a corner. *J Fluid Mech* 1979;93:413–430
20. Stephanoff K: An experimental study of steady and oscillatory flow through a wavy-walled channel (thesis). Oxford, England, Oxford University, 1981
21. Schlichting H: *Boundary Layer Theory.* New York, McGraw-Hill Book Co, 1968
22. Sauren A: Aortic valve histology and its relation with mechanics. *J Biomech* 1980;13:97–104
23. Rainer GW, Christopher RA, Sadler TR Jr, Hilgenberg AD: Dynamic behavior of prosthetic aortic tissue valves as viewed by high-speed cinematography. *Ann Thorac Surg* 1978; 28:274–280
24. Bellhouse BJ: Sections 6.1 and 6.4, in Baen J, Arntzenius AC, Yellin EL (eds): *Cardiac Dynamics.* Boston, Martinus Nijhoff Publishing, 1980, pp 104–107
25. Sarohia V: Experimental investigation of oscillations in flows over shallow cavities. *AIAA J* 1977;15:984–991
26. Oakley CM: Long-term complications of valve replacement. *Br Med J* 1982;284:995–997
27. Riddle JM, Magilligan DJ Jr, Stein PD: Surface morphology of degenerated porcine bioprosthetic valves four to seven years following implantation. *J Thorac Cardiovasc Surg* 1981; 81:279–287
28. Clark RE, Swanson WM: In vitro durability of Hancock model 242 porcine heart valve. *J Thorac Cardiovasc Surg* 1979; 78:277–280
29. Stein PD, Sabbah HN: Turbulent blood flow in the ascending aorta of humans with normal and diseased aortic valves. *Circ Res* 1976;39:58–65
30. Freis E, Heath W: Hydrodynamics of aortic blood flow. *Circ Res* 1964;14:105–116
31. Van Steenhoven AA, Verlaan C, Veenstra P, Reneman R: In vivo cinematographic analysis of behavior of the aortic valve. *Am J Physiol* 1981;240:H286–H292
32. Pinto E, Damani P, Sternber C, Liedtke A: Fine fluttering of aortic valve as demonstrated by aortic valve echocardiograms. *Am Heart J* 1978;95:807–808
33. Stein PD, Sabbah HN, Magilligan DJ Jr, Lakier JB: Mechanism of a musical systolic murmur caused by a degenerated porcine bioprosthetic valve. *Am J Cardiol* 1982;49:1874–1882
34. Ratshin RA, Karp R, Kirklin J, Kouchoukos W, Plalitilo A: Postoperative evaluation of aortic valve homografts using echocardiography (abstract). *Circulation* 1973;48(suppl IV):IV-206
35. Fry DL: Acute vascular endothelial changes associated with increased blood velocity gradients. *Circ Res* 1968;22:165
36. Cornhill J, Roach M: Quantitative study of localization of atherosclerotic lesions in rabbit aorta. *Atherosclerosis* 1976; 23:489–501
37. Weinstein L, Schlesinger J: Pathoanatomic, pathophysiologic and clinical correlations in endocarditis. *N Engl J Med* 1974; 291:832–837


KEY WORDS • hemodynamics • aortic sinus vortex • flow separation • turbulence